P2X7-deficiency improves plasticity and cognitive abilities in a mouse model of Tauopathy

Kevin Carvalho, Elodie Martin, Aurélia Ces, Nadège Sarrazin, Pauline Lagouge-Roussey, Caroline Nous, Leyna Boucherit, Ihsen Youssef, Annick Prigent, Emilie Faivre, et al.

Progress in Neurobiology 206 (2021) 102139

Contents lists available at ScienceDirect

Progress in Neurobiology

journal homepage: www.elsevier.com/locate/pneurobio

Original Research Article

P2X7-deficiency improves plasticity and cognitive abilities in a mouse model of Tauopathy

Kevin Carvalho [a,b], Elodie Martin [c], Aurélia Ces [c], Nadège Sarrazin [c], Pauline Lagouge-Roussey [d], Caroline Nous [d], Leyna Boucherit [d], Ihsen Youssef [c], Annick Prigent [c], Emilie Faivre [a,b], Sabiha Eddarkaoui [a,b], Thibaut Gauvrit [a,b], Didier Vieau [a,b], Susana Boluda [c], Vincent Huin [a,b], Bertrand Fontaine [c,e], Luc Buée [a,b], Benoît Delatour [c], Patrick Dutar [f], Florian Sennlaub [d], Xavier Guillonneau [d], David Blum [a,b,**], Cécile Delarasse [c,d,*], NeuroCEB Brain Bank

[a] University Lille, Inserm, CHU Lille, U1172 – LilNCog – Lille Neuroscience & Cognition, F-59000 Lille, France
[b] Alzheimer & Tauopathies, LabEx DISTALZ, France
[c] ICM Institut du Cerveau, CNRS UMR7225, INSERM U1127, Sorbonne Université, Hôpital de la Pitié-Salpêtrière, Paris, France
[d] Sorbonne Université, INSERM, CNRS, Institut de la Vision, 17 rue Moreau, F-75012 Paris, France
[e] Sorbonne Université, AP-HP, Hôpital Pitié-Salpêtrière, Inserm, CNRS, Institut de myologie, Paris, France
[f] Biophotonics and Synapse Physiopathology, Lumière, Matière et Interfaces (LuMIn), CNRS, ENS Paris-Saclay, Université Paris-Saclay, Centrale Supélec, Gif-sur Yvette, France

ARTICLE INFO

Keywords:
Purinergic receptor
P2X7
Tauopathies
Frontotemporal lobar degeneration
Alzheimer's disease
Chemokines

ABSTRACT

Alzheimer's disease is the most common form of dementia characterized by intracellular aggregates of hyperphosphorylated Tau protein and extracellular accumulation of amyloid β (Aβ) peptides. We previously demonstrated that the purinergic receptor P2X7 (P2X7) plays a major role in Aβ-mediated neurodegeneration but the relationship between P2X7 and Tau remained overlooked. Such a link was supported by cortical upregulation of P2X7 in patients with various type of frontotemporal lobar degeneration, including mutation in the Tau-coding gene, MAPT, as well as in the brain of a Tauopathy mouse model (THY-Tau22). Subsequent phenotype analysis of P2X7-deficient Tau mice revealed the instrumental impact of this purinergic receptor. Indeed, while P2X7-deficiency had a moderate effect on Tau pathology itself, we observed a significant reduction of microglia activation and of Tau-related inflammatory mediators, particularly CCL4. Importantly, P2X7 deletion ultimately rescued synaptic plasticity and memory impairments of Tau mice. Altogether, the present data support a contributory role of P2X7 dysregulation on processes governing Tau-induced brain anomalies. Due to the convergent role of P2X7 blockade in both Aβ and Tau background, P2X7 inhibitors might prove to be ideal candidate drugs to curb the devastating cognitive decline in Alzheimer's disease and Tauopathies.

1. Introduction

Tauopathies are a large group of neurodegenerative diseases characterized by intracellular aggregates of pathological Tau proteins in the central nervous system (Lebouvier et al., 2017). Alzheimer's disease is the most common Tauopathy, characterized by both neuronal accumulations of hyperphosphorylated and aggregated Tau proteins into neurofibrillary tangles and extracellular aggregation of amyloid β (Aβ) peptides into senile plaques. In Alzheimer's disease, the progression of Tau pathology from entorhinal cortex, hippocampus, and finally neocortex corresponds to the progression of clinical symptoms (Brier et al., 2016; Duyckaerts et al., 1997; Grober et al., 1999), suggesting a central role in the cognitive decline. However, pathways underlying Tau pathology-induced cognitive deficits remain ill-defined. Genetic and experimental studies highlighted the significant contribution of immune mechanisms to synaptic and cognitive deficits in Alzheimer's disease and Tauopathies (Ising et al., 2019; Laurent et al., 2016; Laurent et al., 2017; Leyns and Holtzman, 2017; Zotova et al., 2013).

The purinergic receptor P2X7 (P2X7) is a nonselective cationic channel – responding to high amounts of ATP released by damaged or

* Corresponding author at: Inserm, UMRS968, Institut de la Vision, Paris F-75012, France.
** Corresponding author at: Inserm UMRS1172, 'Alzheimer & Tauopathies', Place de Verdun, 59045 Lille Cedex, France.
E-mail addresses: david.blum@inserm.fr (D. Blum), cecile.delarasse@inserm.fr (C. Delarasse).

https://doi.org/10.1016/j.pneurobio.2021.102139
Received 23 March 2021; Received in revised form 6 July 2021; Accepted 6 August 2021
Available online 12 August 2021

activated cells – that has been extensively characterized in the immune system, where it plays major role in the release of pro-inflammatory cytokines, notably IL-1β (Di Virgilio et al., 2017; Ferrari et al., 2006; Solle et al., 2001). In the nervous system, the functions of P2X7 remain however unclear. P2X7 expression was mainly reported in glial cells while neuronal expression remains debated (Kaczmarek-Hajek et al., 2018). In neurological diseases, P2X7 functions may change depending on the physiopathological context, exerting either protective or detrimental roles (Kanellopoulos and Delarasse, 2019; Sperlagh and Illes, 2014). We and others reported a marked upregulation of P2X7 in the brain of Alzheimer's disease patients, notably in microglia and astrocytes surrounding amyloid plaques (Martin et al., 2019; McLarnon et al., 2006). In a transgenic amyloid mouse model of Alzheimer's disease, we noticeably showed that P2X7 is involved in Aβ-induced chemokines

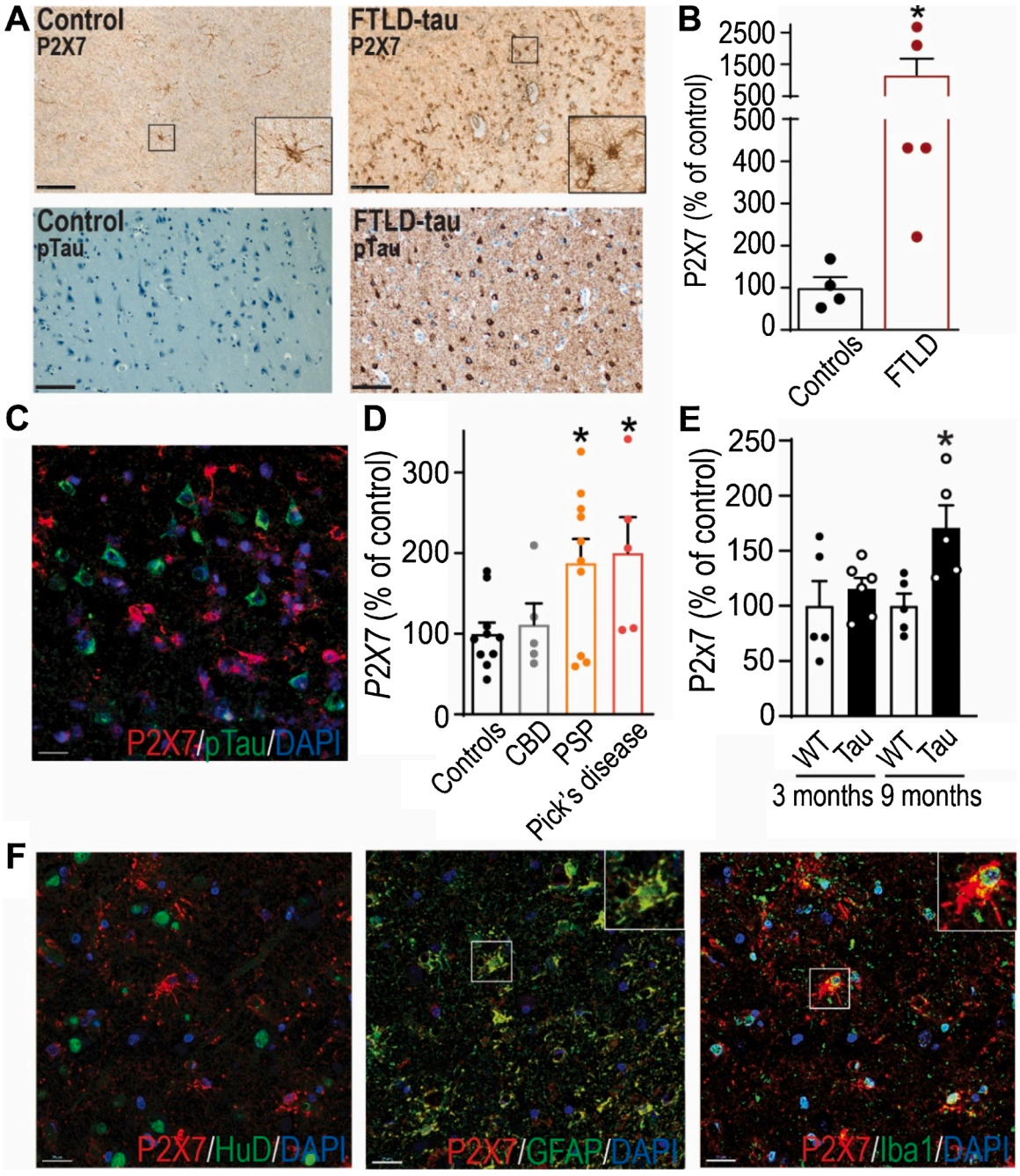

Fig. 1. Increased levels of P2X7 in the brain of patients with Tauopathy and Tau transgenic mice. (A) Representative images of brain sections from non-demented human controls (left column) and FTLD-Tau patients (right column) stained with an anti-P2X7 antibody (upper row) or anti-pTau (AT8) antibody (bottom row). Scale bar: 100 μm. (B) Corresponding quantification of P2X7 staining in the gray matter from non-demented human controls ($n = 4$) and FTLD patients ($n = 5$). Mann Whitney test. *$P < 0.05$. (C). Representative image of brain sections from FTLD-Tau patients, double immunostained with anti-P2X7R (red) and anti-pTau (cloneAT100, green) (D) Quantification of P2X7 mRNA in the brain of non-demented human controls ($n = 10$), CBD ($n = 5$), PSP ($n = 10$) and Pick's disease ($n = 5$) patients. One-way ANOVA followed by Kruskal–Wallis *post hoc* test. *$P < 0.05$ *vs* controls. (E). Quantification of P2x7 mRNA in the hippocampus of 3- and 9-month-old wild-type ($n = 5$) and Tau mice ($n = 5$–6/group). One-way ANOVA followed by Kruskal–Wallis post hoc test. *$P < 0.05$ *vs* controls. (F) Representative images (overview and magnification) of brain sections from FTLD-Tau patients, immunostained with anti-P2X7R (red) and either (left panel) anti-HuD (neuron marker, green) and (right panel) anti-Iba1 (microglial marker, green), or (middle panel) anti-GFAP (astrocyte marker, green) antibodies. Scale bar: 20 μm. (For interpretation of the references to color in this figure legend, the reader is referred to the web version of this article.)

release with its deletion mitigating both brain lesions and cognitive deficits (Martin et al., 2019). In sharp contrast, the link between P2X7 and Tau remains largely ill-defined.

In the present study, we first demonstrated an increased expression of P2X7 in the cortex of human patients with primary Tauopathies including frontotemporal lobar degeneration (FTLD) with P301L mutation in the Tau-coding gene, microtubule associated protein Tau (MAPT), (FTLD-Tau) as well as in the THY-Tau22 (Tau) mouse model of Tauopathy which develop progressive hippocampal Tauopathy associated with cognitive deficits (Schindowski et al., 2006; Van der Jeugd et al., 2013). We further demonstrated that while P2X7-deficiency had a moderate effect on Tau phosphorylation, it improved neuroinflammatory response by reducing microglia activation and related inflammatory markers. Importantly, P2X7 deletion in Tau mice improved long-term synaptic plasticity and hippocampal-dependent spatial memory supporting that targeting the druggable P2X7 is an attractive strategy to improve Tau-induced cognitive deficits in Alzheimer's disease and Tauopathies.

2. Results

2.1. Patients with Tauopathies and Tau transgenic mice show elevated P2X7 brain expression

We have previously shown that P2X7 is upregulated in the brain of Alzheimer's disease patients as well as in the APPPS1 transgenic mouse model of amyloidogenesis (Martin et al., 2019). To get further insights into a potential relationship between P2X7 and Tau pathology development, we analyzed brain tissues from patients with various primary Tauopathies, as well as from a Tau transgenic mouse model, the THY-Tau22 strain (Schindowski et al., 2006). Using immunohistochemistry, we observed significantly higher density of P2X7 in the temporal cortex of patients with FTLD-Tau ($+1073 \pm 507\%$, $p = 0.016$ *vs* controls) as compared to age-matched non-demented human controls ($0.10 \pm 0.04\%$ of tissue stained) (Fig. 1A and B). P2X7 and pTau co-labelling showed expression of P2X7 in brain area actually encompassing neurofibrillary degeneration (Fig. 1C). Additionally, we evaluated P2X7 mRNA levels in the prefrontal cortex for the other Tauopathies, namely corticobasal degeneration (CBD), progressive supranuclear palsy (PSP) and Pick's disease, through quantitative PCR. We observed a significant increase in P2X7 mRNA levels in both PSP ($+87.8 \pm 29.8\%$; $p = 0.015$ *vs* controls) and Pick's disease ($+100.3 \pm 44.5\%$; $p = 0.015$ *vs* controls) as compared to age-matched controls (Fig. 1D). In order to find a suitable preclinical model to study the relationship between P2X7 and Tau, we also evaluated P2X7 mRNA expression in the THY-Tau22 mice, at the ages of 3 and 9 months, when animals display minimal and overt pathological alterations respectively (Van der Jeugd et al., 2013). Interestingly, we observed a significant increase of P2X7 expression in the hippocampus of 9-month-old Tau mice ($+70.5 \pm 20.7\%$; $p = 0.0005$ *vs* WT 9-month-old mice, Fig. 1E), at a time point hippocampal Tau pathology is largely developed and impacts memory performance (Laurent et al., 2016; Schindowski et al., 2006; Van der Jeugd et al., 2013). Using the RNAscope ISH technique, we also compared the level of P2x7 mRNA in the cortex and in the hippocampus of WT *vs* Tau mice. We found a higher P2x7 mRNA expression in the hippocampus of Tau mice where the pathology mainly develops (WT: 4.2 ± 0.2 dots/cell, $n = 21$; Tau: 4.9 ± 0.2 dots/cell, $n = 45$; $P < 0.05$) while no significant difference was found in the cortex exhibiting much less pathology in this mouse model (Fig. S1A–C). In agreement, we observed, using Western Blot, a significant rise of P2X7 protein level in the hippocampus of Tau mice ($+102.9 \pm 29.1\%$; $p = 0.03$ *vs* WT mice, Fig. S1D and E). Finally, to identify the cell type upregulating P2X7, we performed co-immunolabelling in brain tissues from patients with FTLD-Tau using antibodies raised against neurons (HuD), astrocytes (GFAP) and microglia (Iba1) (Fig. 1F). The increased P2X7 immunoreactivity appeared to be limited to glial cells, i.e. astrocytes and microglia. Overall, our results support that P2X7 expression levels correlates with Tau pathology development in the brain of patients with Tauopathy as well as in a Tau transgenic mouse model.

2.2. Consequences of P2X7 deletion on Tau pathology development

To investigate the impact of P2X7 pathological upregulation towards the development of Tau pathology, associated neuroinflammation and memory deficits, we next generated Tau mice deleted for P2X7 (TauP2x7$^{-/-}$). In order to determine the effect of P2X7-deficiency towards the development of hippocampal Tau hyperphosphorylation and aggregation, we performed immunohistochemical and biochemical analysis. We first evaluated Tau misconformation using MC1 immunolabelling and found no significant difference between Tau and TauP2x7$^{-/-}$ mice (Fig. 2A and B). Tau bears more than 80 phosphorylation sites (Sergeant et al., 2008). Providing that higher phosphorylation leads to the shift of Tau to the acidic range, 2D Tau electrophoresis allows a global overview of the distribution of Tau proteins according to their isoelectric points. We therefore performed a 2D gel electrophoresis analysis to evaluate global charge changes of human Tau protein in the hippocampus of Tau mice expressing or not P2X7 and we observed a slight decrease of Tau species in the acidic pH range while basic species are more present in TauP2x7$^{-/-}$ compared to TauP2x7$^{+/+}$ mice (Fig. 2C), suggestive of a reduced phosphorylation. Using 1D electrophoresis and Western blot, we observed a reduction of phosphorylation at Ser262 in TauP2x7$^{-/-}$ mice ($-33.4 \pm 6.5\%$; $P = 0.0072$ *vs* TauP2x7$^{+/+}$; Fig. 2D and E). However, we could not detect changes at other phospho-epitopes including Thr181, Ser199, Ser396 and Ser404 nor changes in Tau total expression. In addition, to study the impact of the P2X7 knockout on Tau aggregation, biochemical fractionation was performed and sarkosyl-soluble/insoluble fractions analyzed. The amount of sarkosyl-insoluble Tau remained similar in TauP2x7$^{+/+}$ and TauP2x7$^{-/-}$ mice (Fig. S2A and B). In line with MC1 immunostaining, pathological phosphorylation at Thr212/Ser214 and Ser422, detected using the AT100 and Ser422 antibodies, remained unaffected in TauP2x7$^{-/-}$ mice. Therefore, P2X7 deficiency slightly modified Tau phosphorylation in the hippocampus of Tau transgenic mice.

2.3. P2X7 deficiency reduces Tau-dependent hippocampal neuroinflammation

Tau mice progressively develop hippocampal neuroinflammation correlated with Tau pathology development (Ising et al., 2019; Laurent et al., 2017), in a similar manner to what is observed in the brain of Alzheimer's disease patients (Ismail et al., 2020; Zotova et al., 2013). This inflammatory response is characterized by activation of astrocytes and microglia, release of pro-inflammatory cytokines and chemokines, and lymphocyte – but not monocyte-infiltration (Carvalho et al., 2019; Laurent et al., 2017). Since P2X7 has been tightly linked to immune response (Di Virgilio et al., 2017), we next determined the impact of P2X7 deficiency towards Tau-induced neuroinflammation (Fig. 3). We evaluated the hippocampal mRNA levels of several inflammatory markers known to be associated with Tau pathology in Tau mice (Laurent et al., 2016; Laurent et al., 2017). As expected, we found elevated mRNA levels of markers of innate immunity (Cd68, Clec7a, Itgax, Tlr2 and Tlr4), astrocytes (Gfap) and proinflammatory chemokines (Ccl3 and Ccl4) in TauP2x7$^{+/+}$ mice as compared with P2x7$^{+/+}$ mice. Strikingly, we were able to show significantly lower levels of microglia-related markers in TauP2x7$^{-/-}$ mice, namely Cd68 ($-58.5 \pm 10.5\%$; $P = 0.019$ *vs* TauP2x7$^{+/+}$), Tlr2 ($-108.9 \pm 27.1\%$; $P < 0.0001$ *vs* TauP2x7$^{+/+}$), Tlr4 ($-44.8 \pm 14.6\%$; $P = 0.003$ *vs* TauP2x7$^{+/+}$) and Ccl4 ($-97.2 \pm 22.9\%$; $P = 0.045$ *vs* TauP2x7$^{+/+}$), suggesting a reduction of Tau-mediated microglia reactivity (Fig. 3A). To gain additional insights, we further evaluated microglial (Iba1) and astroglial (GFAP) immunoreactivities (Fig. 3B and C). Paralleling mRNA experiments showing

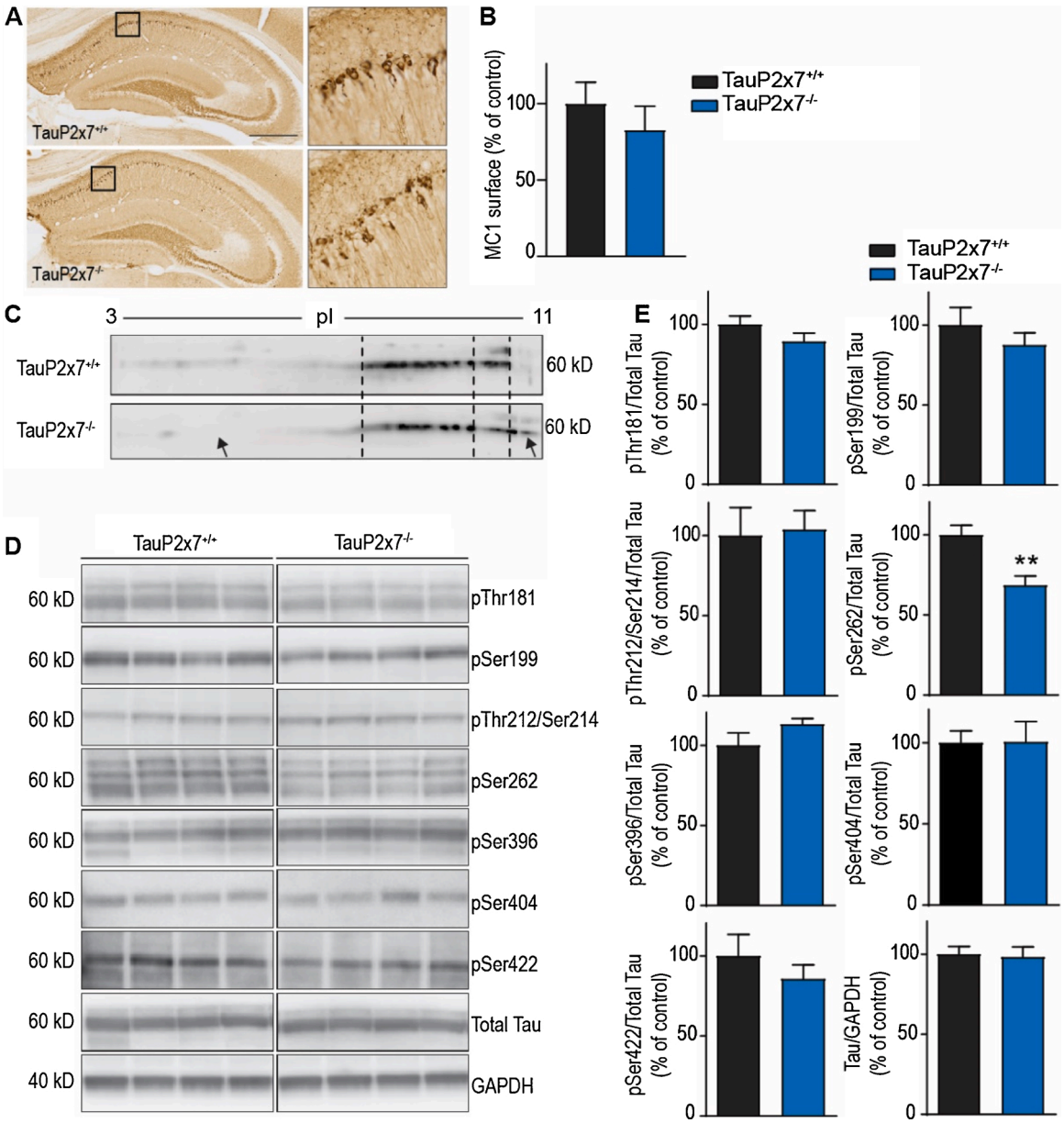

Fig. 2. P2X7-deficiency has no major effect on hippocampal Tau phosphorylation in Tau mice. (A) Representative images (overview in left panels; areas delimited by black insets are magnified in right panels) of brain sections stained with anti-conformational Tau antibody (MC1) in the hippocampus of 8-month-old TauP2x7$^{+/+}$ and TauP2x7$^{-/-}$ mice. (Left panels) Magnifications of areas indicated with black rectangles. Scale bar: 500 µm. (B) Corresponding quantification of MC1 staining in the hippocampus of 8-month-old TauP2x7$^{+/+}$ ($n = 9$) and TauP2x7$^{-/-}$ ($n = 7$) mice. Mann Whitney test. (C) Representative 2D profile of total human Tau (C-ter antibody) in TauP2x7$^{+/+}$ and TauP2x7$^{-/-}$ mice, showing a reduced amount of acidic Tau species and an increase of basic ones in TauP2x7$^{-/-}$ mice (arrows; Total Tau C-ter antibody), suggestive of a reduced phosphorylation. pI (Isoelectric point). (D, E) Representative western blots and quantification of Tau phosphorylation on Thr181, Ser199, Ser212/Thr214, Ser262, Ser396, Ser404 and Ser422 epitopes in TauP2x7$^{+/+}$ and TauP2x7$^{-/-}$ mice ($n = 4$–9 per group). Results are expressed as a percentage of measures obtained in TauP2x7$^{+/+}$ mice. Student's *t*-test. $^{**}P < 0.01$.

reduced glial and immune cells markers after P2x7 invalidation, TauP2x7$^{-/-}$ mice also displayed decreased Iba1-staining in the hippocampus (−24.5 ± 6.8%, $P = 0.027$ *vs* TauP2x7$^{+/+}$) while GFAP remained unaltered. In addition, we determined the number of microglia and the volume occupied by these cells in the hippocampus. We found that the number of Iba1^{+} cells remained similar between TauP2x7$^{+/+}$ (329.3 ± 9.6) and TauP2x7$^{-/-}$ mice (350.9 ± 15.5) while the volume covered by microglia is higher in TauP2x7$^{-/-}$ mice (+26.4 ± 9.2%, $P = 0.035$ *vs* TauP2x7$^{+/+}$) (Fig. 3D) suggestive of a reduced activation. Altogether, these results showed that P2X7-deficiency mitigated microglial activation in Tau pathology, a critical aspect of Tau-mediated neurodegeneration (Carvalho et al., 2019).

2.4. Role of P2X7-dependent CCL4 release in Tau pathology

Based on our observation that TauP2x7$^{-/-}$ expressed a lower level of Ccl4 compared to TauP2x7$^{+/+}$ mice and given that CCL4 was one of the most highly upregulated chemokines in the hippocampus of Tau mice (Laurent et al., 2017), in the cortex of AD patients and amyloid models (Kanellopoulos and Delarasse, 2019), we next investigated whether changes in CCL4 pathway impact Tau pathology in Tau mice. First, to further address the specific role of P2X7 in CCL4 production, we used primary microglial cell cultures from P2x7$^{+/+}$and P2x7$^{-/-}$ mice, stimulated (or not) with the P2X7 agonists, ATP and benzoyl-ATP (Bz-ATP) and analyzed their CCL4 release by ELISA. In line with our *in vivo* results, the levels of CCL4 were significantly lower in the supernatants of

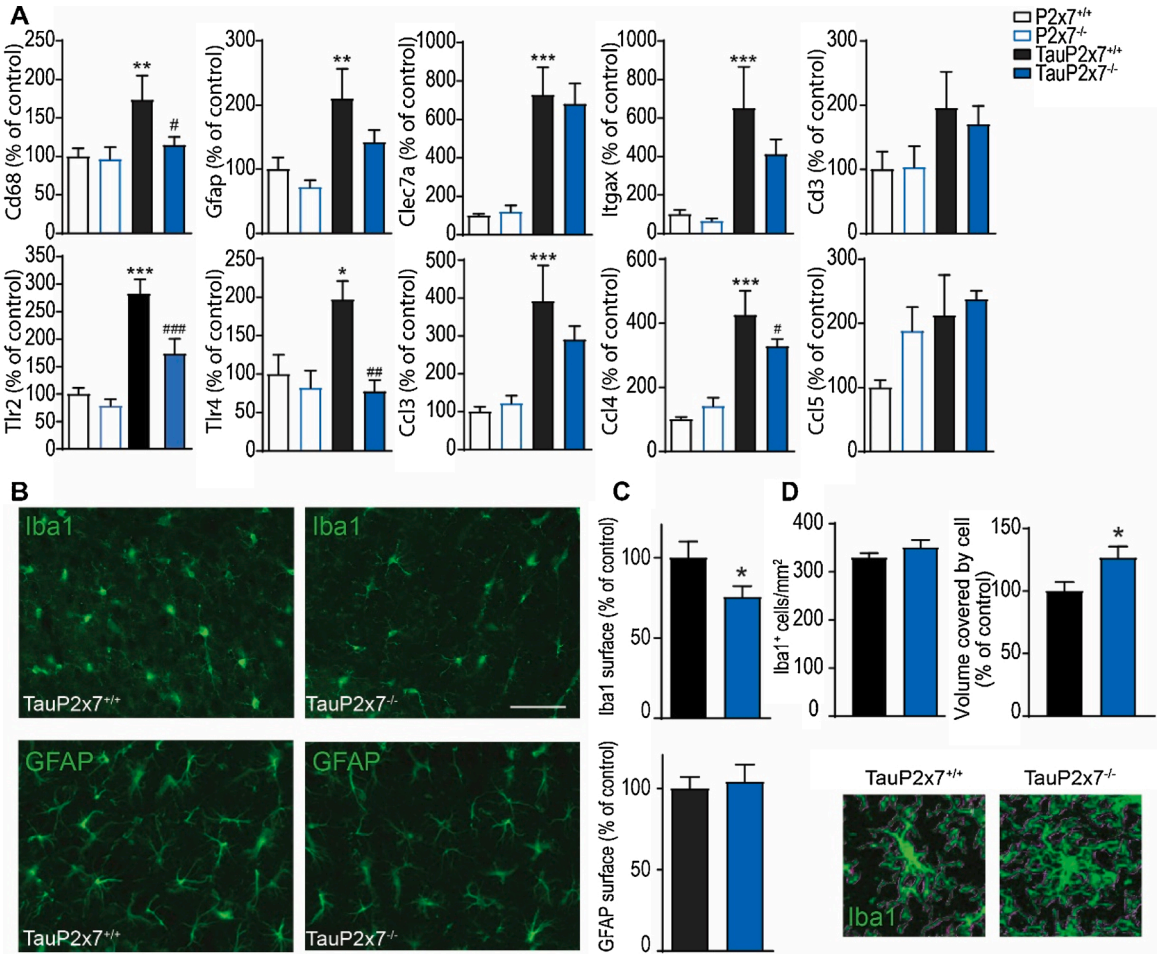

Fig. 3. P2X7-deficiency reduces Tau-related neuroinflammation in Tau mice. (A) qPCR analysis of glial and immune cells markers (Cd68, Gfap, Clec7a, Itgax, Cd3), Toll-like receptors (TLR2 and TLR4) and chemokines (Ccl3, Ccl4 and Ccl5) in the hippocampus of 8-month-old P2x7$^{+/+}$ ($n = 7$–8), P2x7$^{-/-}$ ($n = 5$–6), TauP2x7$^{+/+}$ ($n = 4$), and TauP2x7$^{-/-}$ ($n = 8$–9) mice. One-Way ANOVA followed by a post-hoc Fisher's LSD test. $^{*}P < 0.05$, $^{**}P < 0.01$, $^{***}P < 0.001$ *vs* P2x7$^{+/+}$ and $^{\#}P < 0.05$, $^{\#\#}P < 0.01$, $^{\#\#}\#P < 0.001$ *vs* TauP2x7$^{+/+}$ (B, C) Representative images and quantification of brain slices stained with anti-Iba1 or anti-GFAP in the hippocampus of 8-month-old TauP2x7$^{+/+}$ ($n = 5$–6) and TauP2x7$^{-/-}$ ($n = 6$–7) mice. Scale bar: 50 µm. (D) Quantification of Iba1^{+} positive cells and of the area covered by Iba1^{+} cells in the hippocampus of TauP2x7$^{+/+}$ ($n = 10$) and TauP2x7$^{-/-}$ ($n = 7$) mice. Mann Whitney test. $^{*}P < 0.05$. (Below) Representative images of 3D volume of hippocampal microglia from TauP2x7$^{+/+}$ and TauP2x7$^{-/-}$ mice.

microglial cell cultures from P2x7$^{-/-}$ mice (ATP: 275 ± 48 pg/mL, $P = 0.003$ *vs* P2x7$^{+/+}$; Bz-ATP: 205 ± 6 pg/mL, $P = 0.04$ *vs* P2x7$^{+/+}$; Fig. 4A), compared to those from P2x7$^{+/+}$ mice (ATP: 724 ± 70 pg/mL; Bz-ATP: 370 ± 72 pg/mL; Fig. 4A) indicating the involvement of P2X7 in CCL4 release. Moreover, we addressed, *in vivo*, the role of CCL4 through inhibition of its receptor CCR5 using the potent and selective antagonist maraviroc that crosses the blood–brain barrier (Boffito and Abel, 2008). Since maraviroc does not bind to murine CCR5 (Saita et al., 2007), we used CCR5 knock-in mice expressing human CCR5 (hCCR5ki) crossed with Thy-Tau22 mice. Maraviroc was then administered daily in 6-months-old hCCR5kiTau mice for 2 months when the Tau pathology is already present and still ongoing. The dose of maraviroc administrated to the mice correspond to the high range of the human equivalent dose (975 mg daily for a person of 60 kg) (Nair and Jacob, 2016). Interestingly, we could observe that inhibition of CCR5 with maraviroc reduced Tau phosphorylation at pSer404 and pSer422 in hCCR5kiTau treated with maraviroc (−29.0 ± 2.7%; $P = 0.014$ and −33.4 ± 10.3%; $P = 0.04$) compared to hCCR5kiTau treated with placebo (Fig. 4B and C). These results suggest that P2X7-dependent CCL4 release may contribute in part to Tau pathology.

2.5. P2X7-deficiency rescues cognitive impairment and synaptic dysfunction in Tau mice

We finally investigated whether P2X7-deficiency affects cognitive impairments observed in Tau mice (Van der Jeugd et al., 2013). First, we examined long-term spatial memory using the Morris water maze test. During the training sessions, all mice showed a decrease in the corrected integrated path length over time ($P < 0.001$ for training sessions and no effect of genotype), indicating similar spatial learning abilities between groups (Fig. 5A). Motor function, measured by the velocity of mice across all days, was similar in all groups (Fig. 5B). We next performed a memory probe test. P2x7$^{+/+}$ and P2x7$^{-/-}$ mice exhibited a significant preference for the target quadrant over the non-target quadrants ($P = 0.001$ and $P = 0.001$ respectively) underlining correct memory for the platform location. As expected, TauP2x7$^{+/+}$ mice equally explored all quadrants of the pool ($P = 0.18$), with no spatial preference, indicating major spatial memory alteration. Importantly, TauP2x7$^{-/-}$ mice spent more time in the target quadrant as compared with the other quadrants ($P = 0.002$), emphasizing that P2X7-deficiency prevented memory impairments of Tau mice (Fig. 5C).

We next asked whether improved spatial memory is underlined with changes in hippocampal synaptic plasticity. To address this question, we used ex-vivo electrophysiology in the hippocampus of P2x7$^{+/+}$, P2x7$^{-/}$

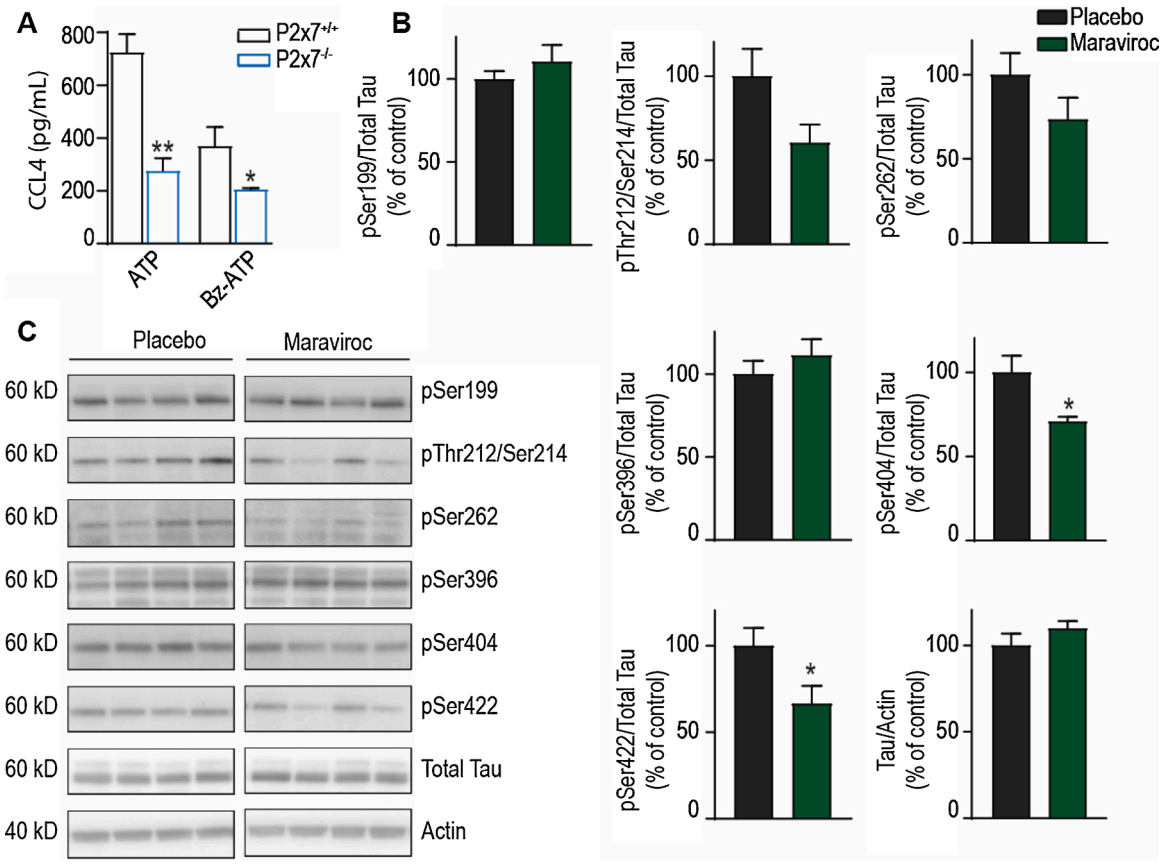

Fig. 4. Effect of pharmacological inhibition of CCR5 on Tau phosphorylation. (A) ELISA results show CCL4 release in primary cultures of microglia from P2x7$^{+/+}$and P2x7$^{-/-}$ mice. Cells were stimulated for 4 h with Bz-ATP (300 μM), or with ATP (1 mM). Student's *t*-test. *$P < 0.05$, **$P < 0.01$. Data are representative of two independent experiments. (B, C) Representative western blots and quantification of Tau phosphorylation on Ser199, Thr212/Ser214, Ser262, Ser396, Ser404 and Ser422 epitopes, as well as dephosphorylated Tau in 8-month-old hCCR5kiTau/Placebo and hCCR5kiTau/Maraviroc mice ($n = 8$ per group). Results are expressed as a percentage of Placebo. Student's *t*-test. **$P < 0.01$.

$^{-}$, TauP2x7$^{+/+}$ and TauP2x7$^{-/-}$ mice. Basal synaptic transmission was evaluated by measures of Input/Output (I/O) curves and of Paired-Pulse Facilitation (PPF). I/O curves were constructed to assess the responsiveness of the AMPAR subtype of glutamate receptors to electrical stimulation in the different groups of mice. They were not statistically different in the three groups (Fig. 5D). In addition, the PPF ratio were comparable in the groups, indicating that there was no change in the probability of glutamate release (Fig. 5E). Long-term potentiation (LTP) induced by theta-burst stimulation was impaired in acute brain slices obtained from TauP2x7$^{+/+}$ mice (120.0 ± 7.7%; $P = 0.015$) as compared with slices from age-matched P2x7$^{+/+}$ mice littermates (149.5 ± 7.2%) (Fig. 5F and G). In contrast, a robust LTP was induced in slices from P2x7$^{-/-}$ and TauP2x7$^{-/-}$ mice with persistent potentiation (131.6 ± 3.1%; $P = 0.07$ and 141.1 ± 6.0%; $P = 0.47$) to a level similar than control mice (Fig. 5F and G). We also compared long-term depression (LTD) induced by low frequency stimulation in slices from TauP2x7$^{+/+}$ and TauP2x7$^{-/-}$ mice. Slices from TauP2x7$^{+/+}$ mice were found unable to maintain LTD (91.4 ± 3.1% of the baseline) while slices from TauP2x7$^{-/-}$ mice developed a robust LTD (75.2 ± 4.2%; $P = 0.009$ (Fig. S3).

3. Discussion

In the present study, we investigated the pathophysiological role of P2X7 in a transgenic mouse model of Tauopathy. We first found an increased expression of P2X7 in the brain of FTLD-Tau patients. We also found increased P2X7 levels in others Tauopathies, PSP and Pick's disease as well as in the hippocampus of transgenic mice developing a Tauopathy supporting a link between Tau pathology and P2X7. P2X7 deficiency mildly affected Tau phosphorylation itself but significantly mitigated Tau-related microglial response resulting in the restoration of long term synaptic plasticity and spatial memory.

P2X7 is a highly regulated protein and its expression is dependent on external stimuli. P2X7 is globally upregulated in neurological diseases (Kanellopoulos and Delarasse, 2019; Martin et al., 2017; Sperlagh and Illes, 2014) as we observed in the brain of FTLD-Tau patients but it may play different roles in neurodegeneration depending on underlying pathological mechanisms. Thus, we analyzed the mechanism underlying the effects of P2X7 deficiency in Tau mice. In this work, we could demonstrate that P2X7 deletion reduced Tau-induced inflammation in the hippocampus of these mice. We previously reported that, in Tau mice, hippocampal Tau pathology is associated with the development of a neuroinflammatory signature characterized by both astrocytic and microglial response, as reported in other Tau models (Laurent et al., 2018; Laurent et al., 2017). We showed that P2X7 deficiency in Tau mice mostly affected microglia with decreased of Iba1 load and modulation of microglia-related genes upregulated in Tau mice (Cd68, Tlr2, Tlr4 and Ccl4) (Fig. 3). These results are consistent with the predominant expression of P2X7 in microglial cells (Kaczmarek-Hajek et al., 2018) and in agreement with findings in an another Tau model, P301S Tau mice, where treatment with the P2X7 antagonist GSK1482160 reduced Tau pathology via modulation of microglial function (Ruan et al., 2020). Interestingly, whereas in this study P2X7 inhibition also improves hippocampal memory impairments, the effect has been associated with a reduced secretion of Tau-containing exosomes while no reduction of microglia activation was found (Ruan et al., 2020). These differences

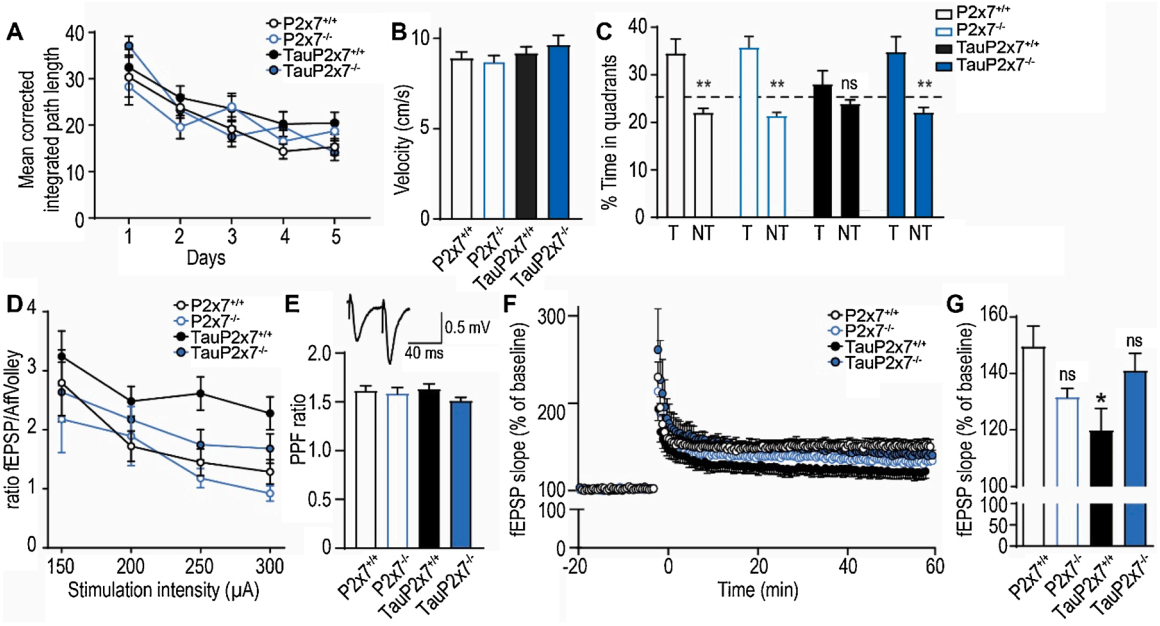

Fig. 5. P2X7-deficiency rescues memory impairments and LTP deficits in Tau mice. (A) Analysis of learning performances in the Morris water maze, assessed with the mean corrected integrated path length taken to reach the hidden platform by 8-month-old P2x7$^{+/+}$ (n = 11), P2x7$^{-/-}$ (n = 10), TauP2x7$^{+/+}$ (n = 11), and TauP2x7$^{-/-}$ (n = 11) mice. Two-way ANOVA with training session and genotype as the principal factors. (B) Velocity of mice in the Morris water maze across all days. One-way ANOVA followed by Kruskal–Wallis post hoc test. (C) Percentage of time spent exploring the target quadrant (TQ) where the platform was previously located *vs* the non-target quadrants (NT) during the memory probe test. P2x7$^{+/+}$ (n = 11), P2x7$^{-/-}$ (n = 10), TauP2x7$^{+/+}$ (n = 12), and TauP2x7$^{-/-}$ (n = 11) mice. t-test. **P < 0.01: difference between T and NT. (D) Mean fEPSP/Afferent Volley slope ratio of synaptic responses plotted against current intensity in 12-month-old P2x7$^{+/+}$ mice (n = 28), P2x7$^{-/-}$ (n = 15), TauP2x7$^{+/+}$ mice (n = 17) and TauP2x7$^{-/-}$ mice (n = 25). Two-way ANOVA with intensity and genotype as the principal factors. (E) Paired-pulse facilitation (PPF) ratio of synaptic transmission in P2x7$^{+/+}$ mice (n = 31), P2x7$^{-/-}$ (n = 27), TauP2x7$^{+/+}$ mice (n = 25) and TauP2x7$^{-/-}$ mice (n = 33). One-way ANOVA followed by Kruskal–Wallis post hoc. Above: representative recording of a PPF in P2x7$^{+/+}$ mouse. (F, G) Long-term potentiation (LTP) during 60 min after application of a theta-burst stimulation. Quantification of the percentage of variation of the fEPSP slope during the LTP maintenance phase, in the last 10 min, in P2x7$^{+/+}$ mice (n = 14), P2x7$^{-/-}$ (n = 14), TauP2x7$^{+/+}$ mice (n = 11) and TauP2x7$^{-/-}$ mice (n = 13). One-way ANOVA followed by Kruskal–Wallis post hoc. *P < 0.05 *vs* P2x7$^{+/+}$ mice.

could be explained by the different phenotypes/time course of the Tau models studied (P301S Tau and THY-Tau22 mice) and the different approaches used to inhibit P2X7.

In Tau mice, Tau pathology development is particularly associated with a progressive upregulation of various microglial inflammatory mediators notably chemokines, complement C1q as well as NLRP3 inflammasome (Carvalho et al., 2019; Ising et al., 2019; Laurent et al., 2017). P2X7-expressing microglia was shown to be involved in pathological processes in several model of neurodegenerative disease via regulation of NLRP3 inflammasome leading to IL-1β secretion (Hu et al., 2015; Kanellopoulos and Delarasse, 2019). In Tau mice, loss of Asc or Nlrp3 decreases Tau pathology and prevents cognitive decline (Ising et al., 2019). However, in TauP2x7$^{-/-}$ mice, we did not observe significant changes in the levels of each component of the Nlrp3 complex (Asc, Nlrp3, Caspase1 & Il-1β) compared to TauP2x7$^{+/+}$ mice (Fig. S4). Similarly, in our previous study, we did not see/highlight any effect of P2X7-deficiency in IL1β release in amyloid mouse model while knockout of Asc or Nlrp3 ameliorated amyloid plaque pathology (Heneka et al., 2013; Martin et al., 2019). Microglia are resident macrophages of the brain with similar activation states. Interestingly, studies by the group of Pelegrin and Surprenant (Pelegrin and Surprenant, 2009) showed that P2X7-downstream signaling depends on the activation state of macrophages. P2X7 induced release of IL-1β from LPS + IFNγ polarized macrophages but not from IL-4-polarized (Pelegrin and Surprenant, 2009). This illustrates clearly that depending on the activation/polarization state of macrophages or microglia, P2X7 activates various signaling pathways (de Torre-Minguela et al., 2016). Overall, synaptic and memory improvements found in TauP2x7$^{-/-}$ mice might be therefore unrelated to NLRP3-dependent regulation in Tau mice. In the same line, while microglia-released C1q has been suggested to mediate Tau-dependent synaptic loss and subsequent memory alterations (Carvalho et al., 2019; Dejanovic et al., 2018), we could not evidence any change in C1q expression in our experiments (data not shown).

Another P2X7-dependent inflammatory process that could be involved in Tau-induced memory impairments is chemokine release. In an amyloid model of Alzheimer's disease, we have shown that P2X7-deficiency affects the release of chemokines CCL3, CCL4, and CCL5 and decrease the recruitment of pathogenic T-cells (Martin et al., 2019). In Tau mice, CCL4 is one of the most highly upregulated chemokines in the hippocampus of Tau mice whose level is tightly correlated to the development of Tau pathology and cognitive deficits (Laurent et al., 2017). CCL4 upregulation has also been described in the cortex of Alzheimer's disease patients and amyloid models (Kanellopoulos and Delarasse, 2019). Interestingly, we found that TauP2x7$^{-/-}$ mice demonstrated reduced CCL4 expression and maraviroc, a competitive antagonist of the CCL4 receptor, reduced Tau pathology supporting that the reduced Tau hyperphosphorylation seen in TauP2x7$^{-/-}$ mice could be, at least in part, ascribed to the reduction of CCL4.

Our data suggest that the primary impact of P2X7 deletion stands at microglial cell level with subsequent neuronal modulation attested by change in phosphorylation of Tau, selectively expressed by neurons in THY-Tau22 mice as well as by improvement of plasticity and spatial memory abilities. In support of this interpretation, in Tau mice, modulation of Tau-induced microglial inflammation was likely associated to the development of synaptic disturbances and memory impairments (Carvalho et al., 2019; Ising et al., 2019; Laurent et al., 2016; Laurent et al., 2017). Moreover, this view is in accordance with recent data obtained in a mouse model of Rett syndrome, a neurodevelopmental disorder, where P2X7-deficiency improves both synaptic and behavioral deficits via reduction of inflammatory cells in the cortex (Garre et al.,

2020). Replacement of the bone-marrow with one from P2X7-deficient mice show that this effect was mainly mediated by the infiltration of macrophages expressing P2X7 and not by yolk-sac derived microglial cells. This is unlikely the case in the present study since, we previously demonstrated the lack of macrophage infiltration in Tau mice and thus the observed effects were mostly related to resident microglia (Laurent et al., 2017).

Microglia plays an essential role in brain development and CNS homeostasis by maintaining the proper function of the neuronal networks (Kierdorf and Prinz, 2017; Salter and Beggs, 2014). Several works showed a direct implication of microglia on synaptic plasticity and memory in the hippocampus. Pro-inflammatory cytokines released by microglia such as IL-1β, IL-6 and TNFα were shown to impair LTP (Jones and Lynch, 2015) and LPS-induced pro-inflammatory cytokines expression in the hippocampus affects hippocampal-dependent spatial memory in old mice (Chen et al., 2008). Mice-deficient for CX3CR1, which is exclusively expressed by microglial cells in the CNS, exhibit impairments in LTP and memory deficits as assessed by Morris water maze (Rogers et al., 2011). Also, conditional deletion of the microglial IL-33 receptor leads to impaired synaptic plasticity and decreased memory precision (Nguyen et al., 2020). Among actors controlling neuro-glial crosstalk that can control plasticity in health and disease, increasing evidence point to purinergic receptors (Salter and Beggs, 2014). For instance, the purinergic microglial receptors P2Y12 were recently showed to be essential for the maintenance of microglia–neuron somatic junctions under physiological conditions (Cserep et al., 2020). Transgenic mice with increased surface density of neuronal P2X4, observed in pathological conditions, exhibited alterations of hippocampal LTD and LTP, and impaired spatial memory (Bertin et al., 2020). Further, upregulation of neuronal A_{2A} receptor in Tau mice leads to synaptic loss in the hippocampus and long term memory impairments linked to modifications of the microglial transcriptional profile (Carvalho et al., 2019). In accordance with such view that purinergic receptors are instrumentally involved on plasticity dysregulations encountered in allostatic conditions, our data support that P2X7-dependent activated microglia participate to Tau-induced synaptic impairments.

Overall, our study is the first showing that P2X7 contributes to the cognitive deficits linked to the development of Tauopathy. This study illustrates once again the complex neuro-glial function of P2X7 in neurodegenerative conditions (Kanellopoulos and Delarasse, 2019). Importantly, our present and previous (Martin et al., 2019) studies highlight that P2X7 deficiency has a major beneficial effect in both amyloid and Tau context. Thus, the pharmacological inhibition of P2X7, impacting both amyloid and Tau-dependent cognitive deficits, needs to be further considered in a translational perspective for patients with Alzheimer's disease and Tauopathies.

4. Materials and methods

4.1. Human brain samples

Post-mortem brain tissues were obtained from the French National Brain Bank, GIE NeuroCEB and brain banks at university medical centers in Lille (France), Paris (France) and Geneva (Switzerland), following approval by the local institutional review board and the provision of written, informed consent by the donor's family. The collection was declared to the Ministry of Research and Higher Education, and the Brain Bank was officially authorized to provide samples to project scientists. The project was approved by the Scientific Committee of the Brain Bank.

For immunohistochemistry, a total of nine post-mortem brain samples (temporal cortex) were used; five from individuals with clinically and neuropathologically diagnosed Frontotemporal lobar degeneration with Tau-coding gene *MAPT* P301L mutation (FTLD-Tau) (Forrest et al., 2018) and four from non-demented controls, neuropathologically free, and, in particular, devoid of Tau-positive lesions (Table S1). Samples were fixed in 10% formalin solution and embedded in paraffin. Brain sections (5-µm thick) were cut on a microtome.

For mRNA analysis, a total of thirty post-mortem brain samples (Brodmann area 10 prefrontal cortex) were used; 20 sporadic FTLD-Tau patients (five corticobasal degeneration, CBD; five Pick's disease and 10 progressive supranuclear palsy, PSP) and 10 other age-matched controls with no signs of cognitive decline, no history of stroke or chronic brain pathology. Most participants and methods have been described previously (Huin et al., 2016) (Table S2). Fresh frozen grey matter tissue (about 100 mg) retrieved at autopsy and stored at −80 °C was used for mRNA analysis.

4.2. Human tissue immunostaining

For immunostaining, brain tissue sections were deparaffinized and pretreated with an antigen retrieval procedure (5 min in citrate buffer at 100 °C in a decloaking chamber) to unmask hidden epitopes. Then, tissue sections were incubated with a goat polyclonal anti-P2X7 antibody (Novus Biologicals, 1/100 dilution) overnight at 4 °C. Sections were then incubated with a secondary biotinylated rabbit anti-goat IgG for 30 min (Vector Labs, 1/250 dilution). Immunoreactivity was detected with the peroxidase-avidin-biotin technique (ABC Elite Kit, Vector Labs) and 3,3′-diaminobenzidine (DAB, Sigma-Aldrich) as the chromogen. Images were acquired with a slide scanner (Nanozoomer, Hamamatsu). In each case, the digitized gray matter of the temporal cortical sample was segmented, based on a fixed [0:230] threshold (ImageJ). Areas that displayed a signal above the threshold were summed and expressed as a percentage of the overall surface area of the cortical ribbon to calculate the P2X7-labeled load.

For immunofluorescence, after antigen retrieval procedure, tissue was permeabilized with 0.2% Triton XT-100 for 10 min. Nonspecific binding was blocked by incubation for 2 h in 4% BSA at room temperature (RT). Sections were then incubated at 4 °C overnight with goat polyclonal anti-P2X7 antibody (Novus Biologicals, 1/100 dilution) in normal horse serum (S2000, Vector Laboratories). After washing with PBS, sections were incubated with normal horse serum (1/100) for 1 h and then with mouse monoclonal anti-pTau antibody (clone AT100, 1/500) and either rabbit polyclonal anti-GFAP antibody (Santacruz, 1/200) or rabbit polyclonal anti-Iba1 antibody (Wako, 1/200) and mouse monoclonal anti-HuD antibody (Santacruz, 1/200) in normal horse serum overnight. Subsequently, sections were incubated with Alexa Fluor 647 donkey anti-mouse, Alexa Fluor 488 donkey anti-rabbit and Alexa Fluor 568 donkey anti-goat secondary antibodies (1/500; Life Technologies) for 1 h at RT. Cell nuclei were stained with DAPI (1/500; Thermofisher) for 10 min and sections were incubated in Sudan Black Buffer (Millipore) for 10 min to reduce tissue autofluorescence. Z-stack images were acquired with a Zeiss scanning confocal microscope equipped with a 40× objective.

4.3. Animals

Mice were treated in accordance with the ARRIVE guidelines for the care and use of experimental animals of the European Union. All procedures were approved by the Regional Ethics Committee and the French Ministry of Research and Higher Education (No. 01118.02). P2X7 knock-out ($P2x7^{-/-}$) mice generated by Gabel's group at Pfizer were obtained from Jackson Laboratory (number 005576) (Solle et al., 2001). THY-Tau22 mice (Tau) express the 4-repeat isoform of human Tau (1N4R) mutated at sites G272 V and P301S under the control of the neuronal Thy1.2 expression cassette (Schindowski et al., 2006). The Tau mice were heterozygous. Heterozygous Tau $P2x7^{+/-}$mice were crossed with $P2x7^{+/-}$ mice to obtain the different groups of mice studied: $P2x7^{+/+}$, $P2x7^{-/-}$, Tau and Tau$P2x7^{-/-}$. $P2x7^{+/+}$ served as control mice. Mice were housed under specific-pathogen-free conditions at the PHENO-ICMice facility of ICM. For the different experiments, we

selected animals at an age that displayed a significant phenotype difference between WT and Tau animals, due to genotype: 8-month-old for histological, biochemical, quantitative-PCR and behavioral experiments and 12-month-old for ex *vivo* electrophysiological experiments. Since no overt gender differences were reported (Laurent et al., 2016), data from both males and females were analyzed as a single group.

Mice expressing human CCR5 (hCCR5ki mice) were generated and provided by Pfizer, Briefly, the hCCR5ki mice were obtained by homologous recombination with the sequence encoding human CCR5 as previously described (Amsellem et al., 2014). The hCCR5ki mice were homozygous. First, Tau mice were crossed with hCCR5ki mice. Their progeny was crossed to obtain hCCR5ki mice (homozygous) and hCCR5ki (homozygous) Tau (heterozygous) mice. Maraviroc, an antagonist of CCR5, was administered 5 days a week during 8 weeks by oral gavage (200 mg/kg). This dose is very well tolerated in mice with no side effect reported (Amsellem et al., 2014). Treatment was started at 6 months of age, an age at which Tau pathology and memory impairments are already significant in Tau mice. hCCR5ki mice served as control mice. All mouse lines had a C57BL/6 background.

4.4. Morris water maze

Spatial memory was evaluated in 7-month-old P2x7$^{+/+}$ (n = 11), P2x7$^{-/-}$ (n = 10), TauP2x7$^{+/+}$ (n = 11), and TauP2x7$^{-/-}$ (n = 11) male mice with the Morris water maze (MWM) paradigm. The MWM relied on a 150-cm diameter pool filled with opacified water (21–22 °C). A 10-cm diameter platform was submerged 0.5 cm below the water surface in the center of one of the pool quadrants. The hidden platform remained at a constant position throughout the trials. Training consisted of one session (4 trials/session; start positions pseudo-randomly varied among the four cardinal points) every day for 5 consecutive days. Each trial ended when the animal reached the platform. The animal had a maximum of 60-s to reach the platform, after which it was manually guided to the platform. Once on the platform, the animal was given a 30-s rest before being returned to its cage. The inter-trial interval was approximately 1 h. On the 6th training session, a probe test was performed. During this memory test, the platform was removed, and the mouse was allowed to freely navigate for 60-s.

Data were collected, analyzed, and stored with Any-Maze software (Stoelting Co., Wood Dale, IL, USA). For assessing learning, we determined the unbiased measure "corrected integrated path length" (CIPL) parameter for each trial, which is the sum of the distances traveled by the mouse, from its start position to the platform, minus the distance the mouse would have traveled, swimming at its mean speed, along the shortest possible path between the start position and the platform (Barnes et al., 1997). During the probe test, the percent of time spent in each quadrant was calculated to evaluate memory-related bias for the platform location.

4.5. Ex vivo electrophysiology

Electrophysiological experiments were performed with 12-month-old mice. Previously described methods were used for generation of hippocampal sections, recordings of presynaptic fiber volleys (PFV) and field excitatory postsynaptic potentials (fEPSPs), construction of Input/Output (I/O) curves and measures of paired-pulse facilitation (PPF) (Potier et al., 2010). Long-term potentiation (LTP) was induced by theta-burst stimulation, consisting of five trains of four 100 Hz pulses each, separated by 200 ms and delivered at the test intensity (repeated four times with an interburst interval of 10 s). Testing with a single pulse was then resumed at 0.33 Hz for 60 min. Long-term depression was induced by applying a low-frequency stimulation at 2 Hz (1200 pulses for 10 min).

4.6. Mouse tissue preparation

For immunohistochemistry, 8-month-old mice were deeply anaesthetized and perfused transcardially with 50 mL of PBS. The brains were removed and fixed by immersion in 4% paraformaldehyde, then cryoprotected. Brains were sliced on a freezing microtome (40 µm serial sections).

For biochemical and mRNA analyses, 8-month-old mice were quickly killed by decapitation, as anesthesia promotes Tau hyperphosphorylation (Planel et al., 2007). The brains were removed from the skulls and snap-frozen.

4.7. Mouse tissue immunostaining

For MC1 immunostaining, free-floating 40 µm sections were incubated overnight at 4 °C with mouse monoclonal anti-MC1 antibodies (Peter Davies, 1/1000 dilution). Then, the sections were incubated with biotinylated goat anti-mouse IgG antibodies for 1 h at room temperature (Vector Labs, 1/400 dilution). MC1 immunoreactivity was detected with the peroxidase-avidin-biotin technique (ABC Elite Kit, Vector Labs) with DAB as the chromogen. The time of revelation in DAB was the same for all tissues. Images were acquired with a slide scanner (Axioscan, Zeiss).

For glial cell immunofluorescence, free-floating 40 µm sections were incubated overnight at 4 °C with anti-Iba1 (Wako, 1/1000 dilution) and anti-GFAP (Dako, 1/1000 dilution) rabbit polyclonal antibodies. Sections were subsequently incubated with the appropriate Alexa Fluor secondary antibodies (Life Technologies, 1/1000 dilution, 2 h at room temperature). Images were acquired with a fluorescent microscope (DM5500, Leica).

Images were quantified for labelled area fraction (%) by automated counting using ImageJ software. Briefly, images were normalized by subtracting background. A fixed [0:160] threshold for MC1 or an automatic thresholding for Iba1 and GFAP was applied as previously described (Martin et al., 2017). Mean values of area fraction (%) were obtained from images of each mouse hippocampus. Z-stack images were acquired with a Zeiss scanning confocal microscope equipped with a 40× objective. The volume covered by Iba1^{+} cells were determined using Imaris software.

4.8. Hippocampal protein homogeneization

Tissue was homogenized in 200 µL Tris buffer (pH 7.4) containing 10% sucrose and protease inhibitors (Complete; Roche Diagnostics), sonicated and kept at −80 °C until use. Protein amounts were evaluated using the BCA assay (Thermo Scientific).

4.9. Western blot analyses

Proteins samples were diluted with lithium dodecyl sulphate buffer (2×) supplemented with reducing agents (Invitrogen) and then separated on Criterion XT Bis-Tris protein gel 4–12% (Bio-Rad). Proteins were transferred to nitrocellulose membranes, which were then saturated with 5% non-fat dry milk or 5% bovine serum albumin in TNT (Tris 15 mM pH8, NaCl 140 mM, 0,05% Tween) and incubated at 4 °C for 24 h with the primary antibodies directed against phosphoepitope of Tau protein as followed: phospho(p)-Thr181 (AT270, Thermo Scientific, 1/1000 dilution), pThr212/pSer214 (AT100) (Thermo Scientific, 1/1000 dilution), pSer199 (Millipore, 1/2000 dilution), pSer262 (Invitrogen, 1/1000 dilution), pSer396 (Invitrogen, 1/10 000 dilution), pSer404 (Invitrogen, 1/10 000 dilution), pSer422 (Invitrogen, 1/2000 dilution), total Tau C-ter (homemade, 1/10 000 dilution), GAPDH (Santa Cruz, 1/10 000 dilution) and Actin (Sigma-Aldrich, 1/10 000). Appropriate HRP-conjugated secondary antibodies were incubated for 1 h at room temperature and signals were visualized using chemiluminescence detection kits (ECL, Amersham Bioscience) and a LAS3000 imaging system (Fujifilm). Results were normalized to Total

Tau or GAPDH and quantifications were performed using ImageJ software.

For sarkosyl-soluble/insoluble protein preparations, hippocampi were homogenized by sonication in a lysis buffer containing 10 mM Tris-HCl, pH 7.4, 0.32 M sucrose, 800 mM NaCl and 1 mM EGTA with protease inhibitors (Complete w/o EDTA, Roche Diagnostics), and centrifuged at 12 000 g for 10 min at 4 °C. The supernatant incubated 1 h in 1% sarkosyl (N-laurylsarkosine sodium salt, Sigma) at room temperature was then centrifuged at 100 000 g for 1 h at 4 °C, thus forming the supernatant and pellet containing sarkosyl-soluble and -insoluble Tau species, respectively. Sarkosyl-insoluble proteins were directly resuspended in LDS 2× and sarkosyl-soluble samples were mixed with LDS 2×, supplemented with reducing agents (Invitrogen). Sarkosyl-soluble and -insoluble samples were loaded onto NuPage Novex (Invitrogen) gels at a ratio of 1:2 (v:v).

4.10. Bi-dimensional electrophoresis

Protein lysates were precipitated with methanol/chloroform. Fifteen micrograms of proteins were dissolved in 2D buffer (7 M urea, 2 M thiourea, 4% CHAPS and 0.6% pharmalytes). Lysates were loaded on immobilized pH gradient strip 3–11 ReadyStrip (Amersham GE) and isoelectrofocused with the Protean IEF cell (Amersham GE) according to the manufacturer's instructions. The strips were layered onto a Criterion XT Bis-Tris protein gel 4–12%, 11 cm IPG/prep (Bio-Rad). Membranes were incubated with total Tau antibody (C-ter).

4.11. mRNA extraction and quantitative PCR analysis

Total mRNA was extracted from hippocampi and purified using the RNeasy Lipid Tissue Mini Kit (Qiagen). One microgram of total RNA was reverse-transcribed using the High-Capacity cDNA reverse transcription kit (Applied Biosystems). Quantitative real-time reverse transcriptase-PCR analysis was performed on Applied Biosystems™ StepOnePlus™ Real-Time PCR Systems using Power SYBRGreen PCR Master Mix (Applied Biosystems) or TaqMan™ Gene Expression Master Mix (Applied Biosystems). The thermal cycler conditions were as follows: 95 °C for 10 min, then 40 cycles at 95 °C for 15 s and 60 °C for 25 s for SYBRGreen; and 95 °C for 10 min, then 40 cycles at 95 °C for 15 s and 60 °C for 1 min for Taqman. Sequences of the primers and reference of Taqman probes used are given in Supplementary Table 1. Cyclophilin A (PPIA) was used as internal control. Amplifications were carried out in duplicate and the relative expression of target genes was determined by the ΔΔCT method.

4.12. RNAscope in situ hybridization (ISH)

RNAscope ISH (Advanced Cell Diagnostics) was performed with 18-μm sections of frozen brain embedded in cryo-embedding medium. Tissues were fixed in 4% paraformaldehyde, and then the slides were processed with the RNAscope multiplex fluorescent assay, according to manufacturer instructions. We used the probes designed by the manufacturer including Mm_P2X7R-C1, and positive and negative controls, Mm-PPIB and DapB (of the Bacillus subtilis strain), respectively. Immunofluorescence images were captured with a Olympus scanning confocal microscope. Quantifications were performed with ImageJ software.

4.13. Primary cell culture and stimulation of chemokine release

Primary cultures of microglia were prepared from the brain hemispheres of 1–3 days old. Cells were grown in culture medium containing DMEM, Glutamax, nonessential amino acids, sodium pyruvate, gentamycin, and 10% endotoxin-free fetal calf serum (Life Technologies). Cells were then plated in 10 cm culture dishes coated with poly-ornithine and incubated at 37 °C in a humid atmosphere with 5% CO2. The medium was changed weekly. After 2 weeks, microglia were recovered from the astrocyte layer by shaking (325 rpm) on an orbital shaker for 1 h at room temperature. Cells were washed and seeded at a density of 50,000 cells/well in 96-well plates. These conditions yielded nearly pure microglia populations. For cell stimulation, the medium was replaced with DMEM containing 0.5% BSA. Then, cells were stimulated with ATP or Bz-ATP (Sigma-Aldrich) for 4 h at 37 °C and 5% CO_2. CCL4 levels in the supernatant were assessed with mouse CCL4 DuoSet ELISAs according to the manufacturer's instructions (R&D Systems).

4.14. Statistics

All data are expressed as the mean ± SEM. Differences between two groups were determined using the Student's *t*-test or Mann Whitney test. Comparisons between several groups were analyzed using two-way analysis of variance (ANOVA) or one-way ANOVA, followed by Kruskal–Wallis or Fisher's LSD post hoc test using GraphPad Prism 8 (GraphPad Software). Each figure legend specifies the statistical test used. Statistical significance was defined as: $^{*}P < 0.05$, $^{**}P < 0.01$, and $^{***}P < 0.001$. Outlier values detected with Grubbs' test (GraphPad Software) were excluded from the analyses. Animals were allocated to experimental groups according to the genotype. Data analyses were performed blinded to the genotype.

Authors' contribution

K.C., B.F., L.B., F.S., X.G., D.B. and C.D. conceptualized the project; K.C., E.M., A.C., N.S., P.L-R, C.N., L.B., I.S., A.P., E.F., S.E., T. G., D. V., B. D., P.D., X. G., D.B. and C.D. performed experiments and analyzed data; S.B., NeuroCEB Brain Bank and V.H. provided human materials; K.C., D. B. and C.D. wrote the manuscript with input from all authors.

Competing interests

No competing interests.

Declaration of Competing Interest

The authors report no declarations of interest.

Acknowledgments

This work was supported by grants from INSERM, Sorbonne University, Agence Nationale pour la Recherche (ANR-12-MALZ-0003-02-P2X7RAD), the Programme Investissements d'Avenir IHU FOReSIGHT (ANR-18-IAHU-01). DB and LB are supported by grants from Hauts-de-France (PARTEN-AIRR, COGNADORA), ANR (ADORASTrAU to DB), CoEN (5008 to DB) and Programs d'Investissements d'Avenir LabEx (excellence laboratory) DISTALZ (Development of Innovative Strategies for a Transdisciplinary approach to ALZheimer's disease). Our laboratories are also supported by Fondation pour la Recherche Médicale, France Alzheimer/Fondation de France, FHU VasCog research network (Lille, France), Fondation Vaincre Alzheimer, Fondation Plan Alzheimer as well as Inserm, CNRS, Université Lille, Lille Métropole Communauté Urbaine, DN2M. The PHENO-ICMice and Histomics facilities are supported by 2 "Investissements d'avenir" (ANR-10-IAIHU-06 and ANR-11-INBS-0011-NeurATRIS) and the "Fondation pour la Recherche Médicale". Neuro-CEB is supported by ARSLA, CSC, France DFT, Fondation ARSEP, Fondation Vaincre Alzheimer, France Parkinson. We thank Joanna Droesbeke for technical assistance with mice experiments.

Appendix A. Supplementary data

Supplementary material related to this article can be found, in the online version, at https://doi.org/10.1016/j.pneurobio.2021.102139.

References

Amsellem, V., Lipskaia, L., Abid, S., Poupel, L., Houssaini, A., Quarck, R., Marcos, E., Mouraret, N., Parpaleix, A., Bobe, R., Gary-Bobo, G., Saker, M., Dubois-Rande, J.L., Gladwin, M.T., Norris, K.A., Delcroix, M., Combadiere, C., Adnot, S., 2014. CCR5 as a treatment target in pulmonary arterial hypertension. Circulation 130, 880–891.

Barnes, C.A., Suster, M.S., Shen, J., McNaughton, B.L., 1997. Multistability of cognitive maps in the hippocampus of old rats. Nature 388, 272–275.

Bertin, E., Deluc, T., Pilch, K.S., Martinez, A., Pougnet, J.T., Doudnikoff, E., Allain, A.E., Bergmann, P., Russeau, M., Toulme, E., Bezard, E., Koch-Nolte, F., Seguela, P., Levi, S., Bontempi, B., Georges, F., Bertrand, S.S., Nicole, O., Boue-Grabot, E., 2020. Increased surface P2X4 receptor regulates anxiety and memory in P2X4 internalization-defective knock-in mice. Mol. Psychiatry.

Boffito, M., Abel, S., 2008. A review of the clinical pharmacology of maraviroc. Introduction. Br. J. Clin. Pharmacol. 65 (Suppl. 1), 1–4.

Brier, M.R., Gordon, B., Friedrichsen, K., McCarthy, J., Stern, A., Christensen, J., Owen, C., Aldea, P., Su, Y., Hassenstab, J., Cairns, N.J., Holtzman, D.M., Fagan, A. M., Morris, J.C., Benzinger, T.L., Ances, B.M., 2016. Tau and Abeta imaging, CSF measures, and cognition in Alzheimer's disease. Sci. Transl. Med. 8, 338, ra366.

Carvalho, K., Faivre, E., Pietrowski, M.J., Marques, X., Gomez-Murcia, V., Deleau, A., Huin, V., Hansen, J.N., Kozlov, S., Danis, C., Temido-Ferreira, M., Coelho, J.E., Meriaux, C., Eddarkaoui, S., Gras, S.L., Dumoulin, M., Cellai, L., Neuro, C.E.B.B.B., Landrieu, I., Chern, Y., Hamdane, M., Buee, L., Boutillier, A.L., Levi, S., Halle, A., Lopes, L.V., Blum, D., 2019. Exacerbation of C1q dysregulation, synaptic loss and memory deficits in tau pathology linked to neuronal adenosine A2A receptor. Brain 142, 3636–3654.

Chen, J., Buchanan, J.B., Sparkman, N.L., Godbout, J.P., Freund, G.G., Johnson, R.W., 2008. Neuroinflammation and disruption in working memory in aged mice after acute stimulation of the peripheral innate immune system. Brain Behav. Immun. 22, 301–311.

Cserep, C., Posfai, B., Lenart, N., Fekete, R., Laszlo, Z.I., Lele, Z., Orsolits, B., Molnar, G., Heindl, S., Schwarcz, A.D., Ujvari, K., Kornyei, Z., Toth, K., Szabadits, E., Sperlagh, B., Baranyi, M., Csiba, L., Hortobagyi, T., Magloczky, Z., Martinecz, B., Szabo, G., Erdelyi, F., Szipocs, R., Tamkun, M.M., Gesierich, B., Duering, M., Katona, I., Liesz, A., Tamas, G., Denes, A., 2020. Microglia monitor and protect neuronal function through specialized somatic purinergic junctions. Science 367, 528–537.

de Torre-Minguela, C., Barbera-Cremades, M., Gomez, A.I., Martin-Sanchez, F., Pelegrin, P., 2016. Macrophage activation and polarization modify P2X7 receptor secretome influencing the inflammatory process. Sci. Rep. 6, 22586.

Dejanovic, B., Huntley, M.A., De Maziere, A., Meilandt, W.J., Wu, T., Srinivasan, K., Jiang, Z., Gandham, V., Friedman, B.A., Ngu, H., Foreman, O., Carano, R.A.D., Chih, B., Klumperman, J., Bakalarski, C., Hanson, J.E., Sheng, M., 2018. Changes in the synaptic proteome in tauopathy and rescue of tau-induced synapse loss by C1q antibodies. Neuron 100, 1322–1336 e1327.

Di Virgilio, F., Dal Ben, D., Sarti, A.C., Giuliani, A.L., Falzoni, S., 2017. The P2X7 receptor in infection and inflammation. Immunity 47, 15–31.

Duyckaerts, C., Bennecib, M., Grignon, Y., Uchihara, T., He, Y., Piette, F., Hauw, J.J., 1997. Modeling the relation between neurofibrillary tangles and intellectual status. Neurobiol. Aging 18, 267–273.

Ferrari, D., Pizzirani, C., Adinolfi, E., Lemoli, R.M., Curti, A., Idzko, M., Panther, E., Di Virgilio, F., 2006. The P2X7 receptor: a key player in IL-1 processing and release. J. Immunol. 176, 3877–3883.

Forrest, S.L., Kril, J.J., Stevens, C.H., Kwok, J.B., Hallupp, M., Kim, W.S., Huang, Y., McGinley, C.V., Werka, H., Kiernan, M.C., Gotz, J., Spillantini, M.G., Hodges, J.R., Ittner, L.M., Halliday, G.M., 2018. Retiring the term FTDP-17 as MAPT mutations are genetic forms of sporadic frontotemporal tauopathies. Brain 141, 521–534.

Garre, J.M., Silva, H.M., Lafaille, J.J., Yang, G., 2020. P2X7 receptor inhibition ameliorates dendritic spine pathology and social behavioral deficits in Rett syndrome mice. Nat. Commun. 11, 1784.

Grober, E., Dickson, D., Sliwinski, M.J., Buschke, H., Katz, M., Crystal, H., Lipton, R.B., 1999. Memory and mental status correlates of modified Braak staging. Neurobiol. Aging 20, 573–579.

Heneka, M.T., Kummer, M.P., Stutz, A., Delekate, A., Schwartz, S., Vieira-Saecker, A., Griep, A., Axt, D., Remus, A., Tzeng, T.C., Gelpi, E., Halle, A., Korte, M., Latz, E., Golenbock, D.T., 2013. NLRP3 is activated in Alzheimer's disease and contributes to pathology in APP/PS1 mice. Nature 493, 674–678.

Hu, S.J., Calippe, B., Lavalette, S., Roubeix, C., Montassar, F., Housset, M., Levy, O., Delarasse, C., Paques, M., Sahel, J.A., Sennlaub, F., Guillonneau, X., 2015. Upregulation of P2RX7 in Cx3cr1-deficient mononuclear phagocytes leads to increased Interleukin-1beta secretion and photoreceptor neurodegeneration. J. Neurosci. 35, 6987–6996.

Huin, V., Deramecourt, V., Caparros-Lefebvre, D., Maurage, C.A., Duyckaerts, C., Kovari, E., Pasquier, F., Buee-Scherrer, V., Labreuche, J., Behal, H., Buee, L., Dhaenens, C.M., Sablonniere, B., 2016. The MAPT gene is differentially methylated in the progressive supranuclear palsy brain. Mov. Disord. 31, 1883–1890.

Ising, C., Venegas, C., Zhang, S., Scheiblich, H., Schmidt, S.V., Vieira-Saecker, A., Schwartz, S., Albasset, S., McManus, R.M., Tejera, D., Griep, A., Santarelli, F., Brosseron, F., Opitz, S., Stunden, J., Merten, M., Kayed, R., Golenbock, D.T., Blum, D., Latz, E., Buee, L., Heneka, M.T., 2019. NLRP3 inflammasome activation drives tau pathology. Nature 575, 669–673.

Ismail, R., Parbo, P., Madsen, L.S., Hansen, A.K., Hansen, K.V., Schaldemose, J.L., Kjeldsen, P.L., Stokholm, M.G., Gottrup, H., Eskildsen, S.F., Brooks, D.J., 2020. The relationships between neuroinflammation, beta-amyloid and tau deposition in Alzheimer's disease: a longitudinal PET study. J. Neuroinflamm. 17, 151.

Jones, R.S., Lynch, M.A., 2015. How dependent is synaptic plasticity on microglial phenotype? Neuropharmacology 96, 3–10.

Kaczmarek-Hajek, K., Zhang, J., Kopp, R., Grosche, A., Rissiek, B., Saul, A., Bruzzone, S., Engel, T., Jooss, T., Krautloher, A., Schuster, S., Magnus, T., Stadelmann, C., Sirko, S., Koch-Nolte, F., Eulenburg, V., Nicke, A., 2018. Re-evaluation of neuronal P2X7 expression using novel mouse models and a P2X7-specific nanobody. Elife 7.

Kanellopoulos, J.M., Delarasse, C., 2019. Pleiotropic roles of P2X7 in the central nervous system. Front. Cell. Neurosci. 13, 401.

Kierdorf, K., Prinz, M., 2017. Microglia in steady state. J. Clin. Invest. 127, 3201–3209.

Laurent, C., Buee, L., Blum, D., 2018. Tau and neuroinflammation: what impact for Alzheimer's disease and tauopathies? Biomed. J. 41, 21–33.

Laurent, C., Burnouf, S., Ferry, B., Batalha, V.L., Coelho, J.E., Baqi, Y., Malik, E., Marciniak, E., Parrot, S., Van der Jeugd, A., Faivre, E., Flaten, V., Ledent, C., D'Hooge, R., Sergeant, N., Hamdane, M., Humez, S., Muller, C.E., Lopes, L.V., Buee, L., Blum, D., 2016. A2A adenosine receptor deletion is protective in a mouse model of tauopathy. Mol. Psychiatry 21, 149.

Laurent, C., Dorothee, G., Hunot, S., Martin, E., Monnet, Y., Duchamp, M., Dong, Y., Legeron, F.P., Leboucher, A., Burnouf, S., Faivre, E., Carvalho, K., Caillierez, R., Zommer, N., Demeyer, D., Jouy, N., Sazdovitch, V., Schraen-Maschke, S., Delarasse, C., Buee, L., Blum, D., 2017. Hippocampal T cell infiltration promotes neuroinflammation and cognitive decline in a mouse model of tauopathy. Brain 140, 184–200.

Lebouvier, T., Pasquier, F., Buee, L., 2017. Update on tauopathies. Curr. Opin. Neurol. 30, 589–598.

Leyns, C.E.G., Holtzman, D.M., 2017. Glial contributions to neurodegeneration in tauopathies. Mol. Neurodegener. 12, 50.

Martin, E., Amar, M., Dalle, C., Youssef, I., Boucher, C., Le Duigou, C., Bruckner, M., Prigent, A., Sazdovitch, V., Halle, A., Kanellopoulos, J.M., Fontaine, B., Delatour, B., Delarasse, C., 2019. New role of P2X7 receptor in an Alzheimer's disease mouse model. Mol. Psychiatry 24, 108–125.

Martin, E., Boucher, C., Fontaine, B., Delarasse, C., 2017. Distinct inflammatory phenotypes of microglia and monocyte-derived macrophages in Alzheimer's disease models: effects of aging and amyloid pathology. Aging Cell 16, 27–38.

McLarnon, J.G., Ryu, J.K., Walker, D.G., Choi, H.B., 2006. Upregulated expression of purinergic P2X(7) receptor in Alzheimer disease and amyloid-beta peptide-treated microglia and in peptide-injected rat hippocampus. J. Neuropathol. Exp. Neurol. 65, 1090–1097.

Nair, A.B., Jacob, S., 2016. A simple practice guide for dose conversion between animals and human. J. Basic Clin. Pharm. 7, 27–31.

Nguyen, P.T., Dorman, L.C., Pan, S., Vainchtein, I.D., Han, R.T., Nakao-Inoue, H., Taloma, S.E., Barron, J.J., Molofsky, A.B., Kheirbek, M.A., Molofsky, A.V., 2020. Microglial remodeling of the extracellular matrix promotes synapse plasticity. Cell 182, 388–403 e315.

Pelegrin, P., Surprenant, A., 2009. Dynamics of macrophage polarization reveal new mechanism to inhibit IL-1beta release through pyrophosphates. EMBO J. 28, 2114–2127.

Planel, E., Richter, K.E., Nolan, C.E., Finley, J.E., Liu, L., Wen, Y., Krishnamurthy, P., Herman, M., Wang, L., Schachter, J.B., Nelson, R.B., Lau, L.F., Duff, K.E., 2007. Anesthesia leads to tau hyperphosphorylation through inhibition of phosphatase activity by hypothermia. J. Neurosci. 27, 3090–3097.

Potier, B., Billard, J.M., Riviere, S., Sinet, P.M., Denis, I., Champeil-Potokar, G., Grintal, B., Jouvenceau, A., Kollen, M., Dutar, P., 2010. Reduction in glutamate uptake is associated with extrasynaptic NMDA and metabotropic glutamate receptor activation at the hippocampal CA1 synapse of aged rats. Aging Cell 9, 722–735.

Rogers, J.T., Morganti, J.M., Bachstetter, A.D., Hudson, C.E., Peters, M.M., Grimmig, B. A., Weeber, E.J., Bickford, P.C., Gemma, C., 2011. CX3CR1 deficiency leads to impairment of hippocampal cognitive function and synaptic plasticity. J. Neurosci. 31, 16241–16250.

Ruan, Z., Delpech, J.C., Venkatesan Kalavai, S., Van Enoo, A.A., Hu, J., Ikezu, S., Ikezu, T., 2020. P2RX7 inhibitor suppresses exosome secretion and disease phenotype in P301S tau transgenic mice. Mol. Neurodegener. 15, 47.

Saita, Y., Kondo, M., Shimizu, Y., 2007. Species selectivity of small-molecular antagonists for the CCR5 chemokine receptor. Int. Immunopharmacol. 7, 1528–1534.

Salter, M.W., Beggs, S., 2014. Sublime microglia: expanding roles for the guardians of the CNS. Cell 158, 15–24.

Schindowski, K., Bretteville, A., Leroy, K., Begard, S., Brion, J.P., Hamdane, M., Buee, L., 2006. Alzheimer's disease-like tau neuropathology leads to memory deficits and loss of functional synapses in a novel mutated tau transgenic mouse without any motor deficits. Am. J. Pathol. 169, 599–616.

Sergeant, N., Bretteville, A., Hamdane, M., Caillet-Boudin, M.L., Grognet, P., Bombois, S., Blum, D., Delacourte, A., Pasquier, F., Vanmechelen, E., Schraen-Maschke, S., Buee, L., 2008. Biochemistry of Tau in Alzheimer's disease and related neurological disorders. Expert Rev. Proteomics 5, 207–224.

Solle, M., Labasi, J., Perregaux, D.G., Stam, E., Petrushova, N., Koller, B.H., Griffiths, R. J., Gabel, C.A., 2001. Altered cytokine production in mice lacking P2X(7) receptors. J. Biol. Chem. 276, 125–132.

Sperlagh, B., Illes, P., 2014. P2X7 receptor: an emerging target in central nervous system diseases. Trends Pharmacol. Sci. 35, 537–547.

Van der Jeugd, A., Vermaercke, B., Derisbourg, M., Lo, A.C., Hamdane, M., Blum, D., Buee, L., D'Hooge, R., 2013. Progressive age-related cognitive decline in tau mice. J. Alzheimer's Dis. 37, 777–788.

Zotova, E., Bharambe, V., Cheaveau, M., Morgan, W., Holmes, C., Harris, S., Neal, J.W., Love, S., Nicoll, J.A., Boche, D., 2013. Inflammatory components in human Alzheimer's disease and after active amyloid-beta42 immunization. Brain 136, 2677–2696.